Journal of Materials Chemistry A

ROYAL SOCIETY OF CHEMISTRY

COMMUNICATION

View Article Online
View Journal | View Issue

Cite this: J. Mater. Chem. A, 2023, 11, 26435

Received 1st September 2023
Accepted 16th November 2023

DOI: 10.1039/d3ta05297d

rsc.li/materials-a

Efficient SF_6 capture and separation in robust gallium- and vanadium-based metal–organic frameworks†

Michelle Åhlén, [a] Yi Zhou, *[bc] Daniel Hedbom, [a] Hae Sung Cho, [bcd] Maria Strømme, [a] Osamu Terasaki [bc] and Ocean Cheung *[a]

Sulfur hexafluoride (SF_6) is a highly potent greenhouse gas (GHG) that is mainly emitted from high-voltage electrical applications. The global warming potential (GWP) of the gas is almost 23 000 times that of CO_2 and therefore, controlling its emission and recovery is of great importance from both an environmental and economic perspective. Solid adsorbents and adsorption-based technology is a cost-effective and energy-efficient pathway to recapture SF_6 from its sources, which usually consist of dilute SF_6 in N_2. Here, we present a group of four highly porous and robust gallium- or vanadium-based metal–organic frameworks (MOFs) with exceptional SF_6 uptake and selectivity. In particular, the novel gallium 1,2,4,5-tetrakis(4-carboxlatephenyl) benzene ($TCPB^{4-}$) MOF (Ga-TBAPy) possesses 1-dimensional channels of suitable size (5.2 × 8.4 Å and 5.3 × 10 Å) to adsorb up to 2.25 mmol g^{-1} of SF_6 at 10 kPa with an excellent SF_6-over-N_2 selectivity of 418. Ga-TCPB also exhibits high chemical stability in aqueous and acidic media as well as in organic solvents. 3D electron diffraction (3D ED) patterns combined with high-resolution electron microscopy images were employed to investigate the structure of these water-stable and cyclable MOF SF_6 adsorbents. Furthermore, this study demonstrates the possibility of using these highly stable MOFs to capture SF_6 from a gas mixture as well as how MOFs can offer an alternative and efficient way to mitigate the global warming contributions from the emission of SF_6.

The rise in global warming and associated climate-related issues has long been connected to the anthropogenic emission of greenhouse gases (GHGs). Six industrially relevant GHGs were specified in the Kyoto Protocol in 1997, namely, carbon dioxide (CO_2), hydrofluorocarbons, methane (CH_4), nitrous oxide (N_2O), perfluorocarbons, and sulfur hexafluoride (SF_6).[1] While accounting for 76% of the total greenhouse gas emissions,[2] CO_2 remains the most abundant of the six GHGs. However, the large global warming potential of SF_6 (22 800 times higher than that of CO_2)[3] and its long atmospheric lifetime (3200 years)[4] pose serious concerns. The compound has found wide use (typically in a mixture with N_2)[5] in electrical systems, particularly in high-voltage systems and switchgear, as well as in the semiconductor industry, due to its excellent dielectric properties, high stability, and low toxicity.[3] The atmospheric concentration of SF_6 has, as a consequence, steadily risen in the last 25 years from 3.5 ppt to 11.32 ppt (as of April 2023)[6] due to the growing electricity demands in both developing and developed countries. Sources of SF_6 emissions were in these places attributed to the handling, leaks, and improper recycling of the gas during maintenance and repair.[7] The recovery, as well as recycling of SF_6, particularly from dilute mixtures, is therefore highly important both from an environmental and economic perspective. Adsorption-based processes using solid nanosorbents, such as zeolites,[8,9] porous carbons,[10,11] and metal–organic frameworks (MOFs),[12,13] have shown great promise as a cost-effective and energy-efficient method for GHG capture and separation.[14] MOFs have garnered particular attention in the last couple of decades due to their rich structural diversity, tunable pore size, and surface chemistry which arise from the arrangement of their discrete building units – organic molecules (linkers) and metal ions/clusters (secondary building units).[12,15] Furthermore, the formation of robust MOFs are highly dependent on how these building units are structured and interact – the geometry and rigidity of the organic linkers, the strength of the coordination bonds in the frameworks, as well as the connectivity of the secondary building units.[16–20] MOFs constructed from rod secondary building units (SBUs) encompass an intriguing category of materials that are characterized by their high

[a]Division of Nanotechnology and Functional Materials, Department of Materials Science and Engineering, Uppsala University, Ångström Laboratory, Uppsala 751 03, Sweden. E-mail: ocean.cheung@angstrom.uu.se

[b]Centre for High-resolution Electron Microscopy (ChEM), School of Physical Science and Technology, ShanghaiTech University, Shanghai 201210, People's Republic of China

[c]Shanghai Key Laboratory of High-resolution Electron Microscopy, ShanghaiTech University, Shanghai 201210, People's Republic of China

[d]Department of Chemistry, Chung-Ang University, Seoul, 06974, Republic of Korea

† Electronic supplementary information (ESI) available: Experimental procedures, crystallographic (CCDC: 2300602–2300604) CIF-files, AIF-files, and characterization details. See DOI: https://doi.org/10.1039/d3ta05297d

stability, which is partially derived from their topological structure.[16] The infinite SBU chains form framework structures that in many cases possess uniform 1-dimensional channels that may be used for efficient diffusion, separation, and adsorption of guest molecules.[21] A number of rod MOFs have been reported to date. These rod MOFs are based on common divalent transition metals, such as cobalt, zinc, copper, manganese, and nickel (*e.g.* MOF-74 [$M_2(C_8H_2O_6)$] (where M denotes the divalent metal cation)[22–25] and MOF-71 [$Co(C_8H_2O_4)(C_3H_7NO)$][26]), or higher valence metals such as aluminum(III) (*e.g.* MIL-53 [$Al(OH)(C_8H_2O_4)$][27] and CAU-10-H [$Al(OH)(C_8H_2O_4)$][28]), gallium(III) (*e.g.* MIL-53 [$Ga(OH)(C_8H_2O_4)$][29] and Ga-fumarate [$Ga(OH)(C_4H_2O_4)$][30]), and vanadium(III/IV) (*e.g.* MIL-68 [$V(OH)(C_8H_2O_4)$][31] and MIL-47 [$VO(C_8H_2O_4)$][27]). Combining the strong coordinative bonds that emerge between high valence metal cations (such as gallium (Ga)- and vanadium (V)) and carboxylate-based linkers with the topological stability, and the uniform channel arrangements of rod structures, is an effective strategy for constructing MOFs with excellent stability as well as exceptional sorption properties for small guest molecules (*e.g.* H_2O, CO_2, SO_2).[32–35] Furthermore, introducing rigid and extended linkers into these structures is one approach for building frameworks with increased pore dimensions while retaining the framework's structural and chemical properties. Such moisture-stable frameworks exhibiting high thermal and chemical stability, as well as a high adsorption selectivity for larger guest molecules, are therefore greatly relevant for many industrial applications wherein a sorbent's long-term performance and lifetime are important from an economic perspective. MOF sorbents proposed for SF_6 capture[36–44] have previously not been shown to exhibit these combined properties. With the aim to construct stable rod MOFs with a suitable pore size for capturing the potent greenhouse gas SF_6, we synthesized four robust and highly porous MOFs using gallium or vanadium with two different rigid tetratopic linkers (Fig. 1a). Solvothermal reactions between $VOSO_4 \cdot xH_2O$ or $Ga(NO_3)_3 \cdot xH_2O$ and H_4TBAPy or H_4TCPB in *N*,*N*-dimethylformamide (DMF) yielded four 3-dimensional porous structures, namely, [V_2O_2(TBAPy)] (V-TBAPy), [V_2O_2(TCPB)] (V-TCPB), [$Ga_2(OH)_2$(TBAPy)] (Ga-TBAPy), and [$Ga_2(OH)_2$(TCPB)] (Ga-TCPB) (Fig. 1b–e and S15–S16, S21†). The crystal structure of the MOFs was determined by 3-dimensional electron diffraction (3D ED) (Fig. S1–S8 and Table S1†). The presence of twinning on Ga-TBAPy prevented the direct determination of the framework structure, however, due to its shared similarities with V-TBAPy, a structure model of Ga-TBAPy was built based on the solved structure of V-TBAPy. In brief, the V(IV) metal ions in V-TBAPy was replaced by Ga(III) ions for Ga-TBAPy, and the entire structure was geometry optimized based on the cell parameters obtained by Le Bail refinement against PXRD data (Fig. S14†) of Ga-TBAPy. Low-dose high resolution transmission electron microscope (HRTEM) images were also collected to verify these structures. As shown in Fig. 1c and S1, S3, S5, and S7,† the pore structures were clearly observed in the HRTEM images and matched well with structure models. The four as-synthesized MOFs crystallized in either a monoclinic *P*2/*m* (V-TBAPy, Ga-TBAPy, and Ga-TCPB) or an orthorhombic *Pcma* space group (V-TCPB) with comparable unit cell dimensions aside from unit cell length along the *c*-axis (15.638 Å, 16.095 Å, 21.590 Å, and 10.970 Å for V-TBAPy, Ga-TBAPy, V-TCPB, and Ga-TCPB, respectively) (Table S1†). The

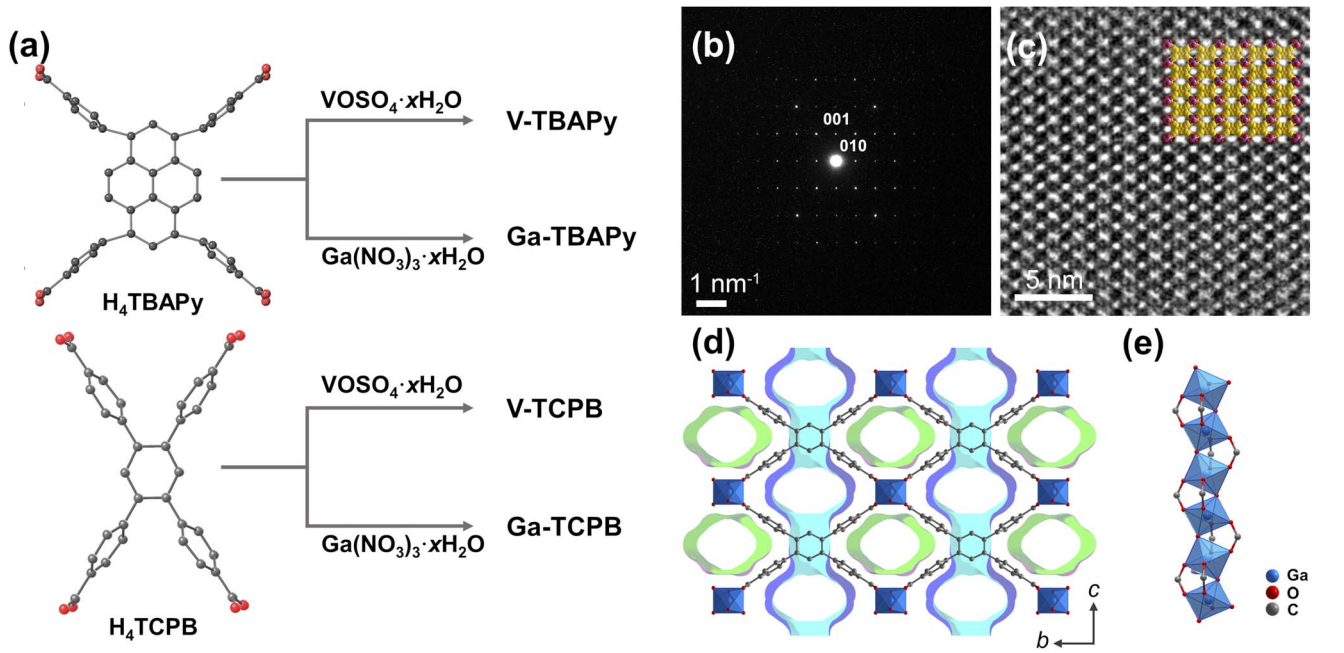

Fig. 1 (a) Synthesis route of Ga- and V-based MOFs with the respective tetratopic H_4TBAPy and H_4TCPB ligands, (b) selected area electron diffraction (SAED) image of Ga-TCPB along [100], (c) corresponding HRTEM image with an insert of the crystal structure of Ga-TCPB as viewed along the *a*-axis, (d) structure of Ga-TCPB as viewed along the *a*-axis showing the presence of two unique pores (colored in green and blue), and (e) the rod SBU running along the *a*-axis in the structure.

structure of the MOFs shared similarities with other TBAPy- and TCPB-based framework structures such as ROD-7 ([$In_2(OH)_2$(TBAPy)]),[45] ACM-1 ([TiO_2(TBAPy)]),[46] CAU-9 ([$Al_2(OH)_2$(TCPB)]),[47] and Sc-CAU-9-TCPB ([$Sc_2(OH)_2$(TCPB)]),[48] which contain rod SBUs consisting of infinite chains of trans corner-sharing octahedra. The Ga(III) and V(IV) metal ions (Fig. S17 and Table S6†) in the structures are coordinated to four different carboxylate groups from the $TBAPy^{4-}$ or $TCPB^{4-}$ linkers and are connected to adjacent metal ions through two bridging μ_2-hydroxide or μ_2-oxo groups in the inorganic chain. The resulting frameworks thus possess two types of 1-dimensional rhombohedral channels propagating along [100] (Fig. 1d and S10–S13†) – a larger channel with dimensions of approximately 5.3–7.9 × 9.5–10 Å and a smaller one 4.9–5.5 Å × 8.4–10 Å, as well as narrow pores (approx. 3.1 Å–3.4 Å) in the [010] direction (taking the van der Waals radii of the atoms into account). The TCPB-based MOFs were found to possess channels of narrower dimensions (approx. 5.2 Å × 10 Å, Fig. S12–S13†) which are of suitable size to host larger greenhouse gas molecules such as SF_6 (kinetic diameter of 5.5 Å). The structural stability of the MOF materials in the presence of external stimuli (*e.g.* temperature) and different chemical environments play a pivotal role in their utilization as sorbents in real-life applications, particularly relating to operating conditions and sorbent handling as well as lifetime. The as-synthesized TCPB-MOFs showed excellent stability in acidic and neutral aqueous media as well as in both protic and aprotic organic solvents at ambient temperatures, while the TBAPy-MOFs were found to be unstable in acidic solutions (Fig. S18 and S19†). The stability of the frameworks is derived from the strong V–O and Ga–O coordinative bonds in the frameworks in conjunction with the shape of the inorganic building units and pore structure. This may in turn lower solvent accessibility, metal–oxygen bond susceptibility for hydrolysis as well as linker dissociation.[49,50] Complete dissolution of the TCPB-based frameworks was only observed in the presence of strong bases such as 0.1 M NaOH. Furthermore, all frameworks also showed high thermal stabilities up to 350 °C and 450 °C for the V- and Ga-based MOFs, respectively (Fig. S20†).

The porosity of the TBAPy- and TCPB-MOFs was confirmed by N_2 sorption at 77 K (Fig. 2a). All four MOFs showed high Brunauer–Emmett–Teller (BET) surface areas between 1107–1484 $m^2\ g^{-1}$ (Fig. S22–S25 and Table S7†). The density functional theory pore size distributions (DFT-PSD) showed the presence of two types of primary pores as identified by the N_2 isotherms (Fig. S22–S25 and Table S7†) ranging in size from 6.0–8.6 Å and 5.4–7.0 Å in the TBAPy- and TCPB-based MOFs, respectively. Taking into account the errors in the calculated DFT-PSDs, arising from deviations between the utilized DFT model and experimental data, the estimated pore apertures

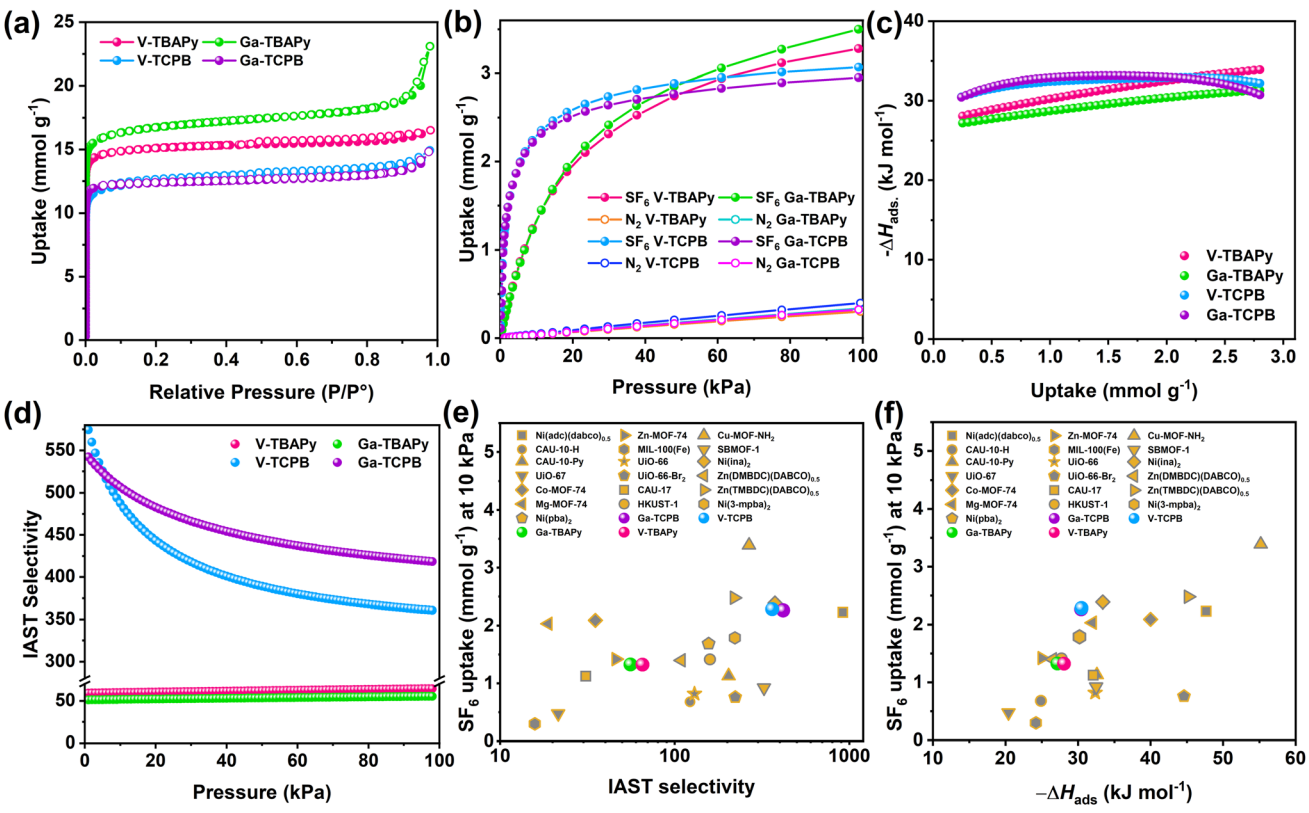

Fig. 2 (a) N_2 sorption isotherms recorded at 77 K (filled and open circles denote the adsorption and desorption branches, respectively), (b) SF_6 and N_2 adsorption isotherms recorded at 293 K, plots of (c) the isosteric enthalpies of SF_6 adsorption ($-\Delta H_{ads}$), and (d) IAST selectivities, and comparisons between SF_6 uptake capacities at 10 kPa and (e) IAST selectivities, (f) $-\Delta H_{ads}$ (at zero or low coverage) of the synthesized TBAPy- and TCPB-MOFs and other porous sorbents.

were comparable with the dimensions of the 1-dimensional channels running along [100] in the crystal structures. The narrow channels along [010] and [001] were not detected due to the kinetic diameter of the N_2 molecules exceeding the size of the pores (approx. 3.0–3.5 Å). The adsorption properties of the TBAPy- and TCPB-MOFs were further investigated using SF_6 and N_2 as well as other well-known greenhouse gases, *i.e.* CO_2, and CH_4 at pressures up to 100 kPa and at 293 K (Fig. 2b and S26†). All four MOFs showed preferential uptake towards the greenhouse gases, especially SF_6 over N_2. The CO_2, CH_4, and N_2 adsorption isotherms (Fig. S26†) of the MOFs showed a linear uptake with increasing pressure (2.83–3.49 mmol g^{-1}, 0.88–1.38 mmol g^{-1}, and 0.30–0.40 mmol g^{-1} at 100 kPa, respectively). This observation signifies a moderate to low affinity between the frameworks and the CO_2 as well as CH_4 and N_2 molecules, which indicates that the pore dimensions are unsuitable for the selective capture of these small molecules (<3.8 Å). However, in regards to SF_6, the TBAPy-based MOFs had the highest SF_6 uptake at 100 kPa of 3.50 mmol g^{-1} and 3.28 mmol g^{-1} for Ga-TBAPy and V-TBAPy, respectively, followed by 3.07 mmol g^{-1} and 2.95 mmol g^{-1} for V-TCPB and Ga-TCPB. These numbers correspond well with the overall decrease in pore volume from the TBAPy- to TCPB-based MOFs. Notably, the shape of the SF_6 isotherm over the pressure range differs significantly between the TBAPy- and TCPB-MOFs (Fig. 2b). The TCPB-MOFs adopt Langmuir-shaped isotherms that approach their apparent saturation capacities at lower pressures as compared to the TBAPy-MOFs for which the SF_6 uptake capacities can be observed to steadily increase with pressure. These differences are attributed to the structural dissimilarities between the TBAPy- and TCPB-linkers (Fig. S9†) in which the benzene-core of the TCPB-linker contracts the channel dimensions along [100], resulting in a reduction in pore volume and an increased affinity between the framework and SF_6 molecules. Correspondingly, the SF_6 uptake capacities of the TCPB-MOFs at 10 kPa (2.29 mmol g^{-1} and 2.26 mmol g^{-1} in V- and Ga-TCPB), were significantly higher than their TBAPy-counterparts (1.33 mmol g^{-1} in both V- and Ga-TBAPy). Furthermore, the SF_6 uptakes of Ga- and V-TCPB were comparable to other high-performing MOFs such as Co-MOF-74 (2.09 mmol g^{-1}),[38] Ni(adc)(dabco)$_{0.5}$ (2.23 mmol g^{-1}),[51] and Ni(ina)$_2$ (2.39 mmol g^{-1})[43] but lower than Cu-MOF-NH_2 (3.39 mmol g^{-1})[44] at 10 kPa and 298 K (Fig. 2e, f and Table S9†). The SF_6 occupancy per unit cell in the MOFs subsequently reached values of 2.59, 2.90, 4.22 and 2.09 for V-TBAPy, Ga-TBAPy, V-TCPB, and Ga-TCPB, respectively, and corresponding SF_6 densities of 860 g L^{-1}, 764 g L^{-1}, 929 g L^{-1}, and 919 g L^{-1} which equates to 126–154 times the density of gaseous SF_6 (6.04 g L^{-1} at 293 K and 101.325 kPa). The SF_6 occupancy per unit cell for V-TCPB is nearly twice that of Ga-TCPB due to the former MOF crystallizing in a different crystal system and thus possessing a larger unit cell. The SF_6 densities in the MOFs imply a high affinity between the framework and SF_6 molecules as well as efficient packing of the SF_6 molecules in the channels of the structures. The guest–host interaction was further evaluated by their isosteric enthalpies ($-\Delta H_{ads}$) of SF_6 adsorption (Fig. 2c). The $-\Delta H_{ads}$ at low coverage (*i.e.* 0.24 mmol g^{-1}) was calculated to be 27–30 kJ mol^{-1} which is comparable to other proposed SF_6 sorbents (Fig. 2f). The $-\Delta H_{ads}$ furthermore increased to 31–34 kJ mol^{-1} in the TBAPy-based MOFs while it remained comparatively constant (31–32 kJ mol^{-1}) in the TCPB-based frameworks as the SF_6 coverage increased to 2.80 mmol g^{-1}. This increase in $-\Delta H_{ads}$ is indicative of growing lateral SF_6–SF_6 interactions which occur as the SF_6 coverage in the channels of the TBAPy-based frameworks increases, while the unchanging $-\Delta H_{ads}$ imply that the adsorption sites and SF_6–SF_6 interactions in V- and Ga-TCPB are energetically similar.[52–54] Overall the calculated $-\Delta H_{ads}$ at both low- and high-coverage is moderate but typical for physisorption processes, thus implying that the sorbents may be regenerated at mild conditions.

Differences in guest–host interactions between SF_6 and N_2 molecules are apparent from the adsorption isotherms (Fig. 2b) for which the gradient of the isotherms, as well as the total N_2 uptake capacities (0.30–0.40 mmol g^{-1} at 293 K and 100 kPa), are significantly smaller for N_2 as compared to SF_6 and furthermore implies a high adsorption selectivity of SF_6 over N_2. The Henry's constants (K_H) of SF_6 and N_2 (Fig. S30 and Tables S12–15†), which corresponds to the partition of the adsorbate between the adsorbed phase and bulk phase in the Henry's regime (*i.e.* low pressures), show SF_6 values 50 to 400 times higher than that of N_2. The Henry's law SF_6-over-N_2 ideal selectivities range from 47.5 (Ga-TBAPy), 53.8 (V-TBAPy) to 365 (V-TCPB) and 437 (Ga-TCPB), further indicating the excellent separation performance of, in particular, the TCPB-based MOFs at low pressures. Furthermore, ideal adsorption solution theory (IAST) selectivities of the MOFs were evaluated by considering a gas mixture composed of SF_6/N_2 at a ratio of 10 : 90. A significant difference between the performance of the TBAPy- and TCPB-based MOFs was observed (Fig. 2d) – the TBAPy-based MOFs exhibited fairly low IAST selectivities of 55 (Ga-TBAPy) and 65 (V-TBAPy) while high selectivities of 361 (V-TCPB) and 418 (Ga-TCPB) were observed for the TCPB-based MOFs at 100 kPa and 293 K. Neither the TBAPy- or TCPB-based MOFs outperform high-performing MOFs such as Cu-MOF-NH_2 (3.39 mmol g^{-1} SF_6 uptake at 10 kPa, 298 K and SF_6/N_2 IAST selectivity of 266.2 at 100 kPa)[44] and Ni(adc)(dabco)$_{0.5}$ (2.23 mmol g^{-1} SF_6 uptake at 10 kPa, 298 K and SF_6/N_2 IAST selectivity of 989.0 at 100 kPa)[51] in terms of SF_6 uptake capacity at 10 kPa nor adsorption selectivity. However, it is crucial to highlight that the combined sorbent properties determine their practical application. Ga-TCPB exhibits a high SF_6 uptake capacity above 2.20 mmol g^{-1} at 10 kPa, SF_6/N_2 IAST selectivity greater than 400, and $-\Delta H_{ads}$ of SF_6 adsorption below 40 kJ mol^{-1} indicating a low energy penalty for sorbent regeneration, as well as excellent thermal- and chemical stability in aqeous and acidic environments. These combined properties make Ga-TCPB unique among sorbents reported for SF_6 capture, to our knowledge, and presents it as a highly promising material for SF_6 capture and separation.

Aspects regarding a sorbent's hydrophilic characteristics are also important to consider particularly in regard to handling and for applications using gas mixtures containing water vapor. The TBAPy- and TCPB-based MOFs generally exhibit low water uptake capacities which is attributed to the hydrophobic

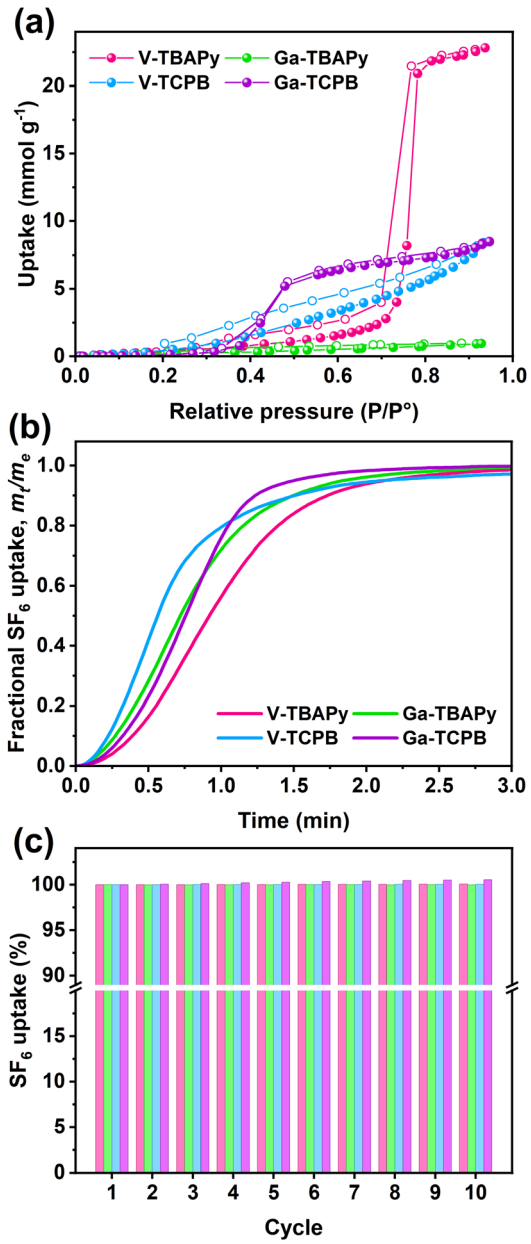

Fig. 3 (a) Water sorption isotherms recorded at 293 K (solid and open spheres represent the adsorption and desorption branches, respectively), (b) gravimetric SF_6 adsorption profiles recorded at 303 K, 100 kPa, and (c) gravimetric SF_6 adsorption cycles.

structure of the TBAPy- and TCPB-linkers (Fig. 3a), in particular, Ga-TBAPy (0.95 mmol g^{-1}, 0.02 g g^{-1} at $P/P^{\circ} = 0.93$) and V-TCPB (8.40 mmol g^{-1}, 0.15 g g^{-1} at $P/P^{\circ} = 0.93$) display linear isotherm shapes throughout the partial pressure range. The water sorption isotherms for V-TBAPy (22.81 mmol g^{-1}, 0.41 g g^{-1} at $P/P^{\circ} = 0.93$) and Ga-TCPB (8.48 mmol g^{-1}, 0.15 g g^{-1} at $P/P^{\circ} = 0.93$), on the other hand, display a Type V shape which has been observed for other microporous MOFs possessing rod-like SBUs such as CAU-10-H[55] and MIL-53.[56,57] The lack of hysteresis in the sorption isotherms furthermore indicates that the adsorption process in all MOFs proceeds without changes, distortion, or degradation of the frameworks,[58] further supporting our previous observations that the structures remain stable in humid environments. Adsorption kinetics and sorbent cycling stability are two other parameters that are important to evaluate in order to assess a sorbent's performance. The TCPB-based MOFs were found to display more rapid SF_6 adsorption as compared to their TBAPy counterparts (Fig. 3b) – reaching 80% of their total uptake capacities within 1 min and 1.2–1.4 min, respectively. Furthermore, all MOFs showed excellent recyclability (Fig. 3c) with a negligible decrease in SF_6 uptake capacity from the first cycle to the tenth cycle.

In summary, we have reported on four highly porous gallium- and vanadium-based rod MOFs containing two different tetratopic linkers – $TBAPy^{4-}$ and $TCPB^{4-}$. These structures were shown to possess 1-dimensional channels approx. 5.3–7.9 × 9.5–10 Å and 4.9–5.5 Å × 8.4–10 Å in dimensions suitable for SF_6 capture. Structural differences between the TBAPy- and TCPB-based linkers were found to impart a narrower pore size in the V- and Ga-TPCB MOFs. The narrow pores enhanced the affinity between the frameworks and the SF_6 molecules, as compared to the TBAPy-MOFs. In particular, Ga-TCPB exhibited an excellent SF_6 uptake capacity of 2.25 mmol g^{-1} at 10 kPa and a high SF_6/N_2 IAST selectivity above 400. The MOF also displayed a moderately low $-\Delta H_{ads}$ below 40 kJ mol^{-1} which in combination with the great thermochemical stability and recyclability of the material renders it as a highly promising sorbent for SF_6 capture. Utilizing robust rod MOFs containing high valence metals and extended tetratopic linkers to both increase guest–host interactions and framework stability is, to our knowledge, unique among reported SF_6 sorbents, and is a highly promising strategy for constructing materials suited for practical applications.

Conflicts of interest

There are no conflicts to declare.

Acknowledgements

The authors thank the Swedish Foundation for Strategic Environmental Research (Mistra) (Project Name: Mistra TerraClean, Project number 2015/31), the Swedish Research Council (Grant No. 2020-04029 and No. 2019-03729) and Swedish Research Council for Sustainable Development (FORMAS, Grant No. 2018-00651) for their financial support. We also acknowledge Myfab Uppsala for providing facilities and experimental support. Myfab is funded by the Swedish Research Council (2019-00207) as a national research infrastructure. This work was also supported by the Center for High-resolution Electron Microscopy (CħEM), ShanghaiTech University (EM02161943), Shanghai Science and Technology Plan (21DZ2260400).

Notes and references

1 D. Liu, X. Guo and B. Xiao, *Sci. Total Environ.*, 2019, **661**, 750–766.
2 S. Akdag and H. Yildirim, *Heliyon*, 2020, **6**, e03396.

3 W.-T. Tsai, *J. Fluorine Chem.*, 2007, **128**, 1345–1352.
4 P. Forster, V. Ramaswamy, P. Artaxo, T. Berntsen, R. Betts, D. W. Fahey, J. Haywood, J. Lean, D. C. Lowe, G. Myhre, J. Nganga, R. Prinn, G. Raga, M. Schulz and R. Van Dorland, *Changes in Atmospheric Constituents and in Radiative Forcing*, Cambridge, United Kingdom and New York, NY, USA, 2007.
5 L. G. Christophorou and R. J. Van Brunt, *IEEE Trans. Dielectr. Electr. Insul.*, 1995, **2**, 952–1003.
6 *Trends in Atmospheric Sulfur Hexafluoride*, **https://gml.noaa.gov/ccgg/trends_sf6/**, (accessed 28 August, 2023).
7 B. K. Sovacool, S. Griffiths, J. Kim and M. Bazilian, *Renewable Sustainable Energy Rev.*, 2021, **141**, 110759.
8 S. Prodinger, R. S. Vemuri, T. Varga, P. B. McGrail, R. K. Motkuri and M. A. Derewinski, *New J. Chem.*, 2016, **40**, 4375–4385.
9 O. Cheung, Z. Bacsik, Q. Liu, A. Mace and N. Hedin, *Appl. Energy*, 2013, **112**, 1326–1336.
10 H. Zhang, Z. Wang, X. Luo, J. Lu, S. Peng, Y. Wang and L. Han, *Front. Chem.*, 2019, **7**, 00919.
11 S. Jung, Y.-K. Park and E. E. Kwon, *J. CO_2 Util.*, 2019, **32**, 128–139.
12 M. Ding, R. W. Flaig, H.-L. Jiang and O. M. Yaghi, *Chem. Soc. Rev.*, 2019, **48**, 2783–2828.
13 R. Aniruddha, I. Sreedhar and B. M. Reddy, *J. CO_2 Util.*, 2020, **42**, 101297.
14 A. Dong, D. Chen, Q. Li and J. Qian, *Small*, 2023, **19**, e2201550.
15 R. L. Siegelman, E. J. Kim and J. R. Long, *Nat. Mater.*, 2021, **20**, 1060–1072.
16 F. M. Amombo Noa, M. Abrahamsson, E. Ahlberg, O. Cheung, C. R. Göb, C. J. McKenzie and L. Öhrström, *Chem*, 2021, **7**, 2491–2512.
17 X.-L. Lv, S. Yuan, L.-H. Xie, H. F. Darke, Y. Chen, T. He, C. Dong, B. Wang, Y.-Z. Zhang, J.-R. Li and H.-C. Zhou, *J. Am. Chem. Soc.*, 2019, **141**, 10283–10293.
18 T. He, X.-J. Kong and J.-R. Li, *Acc. Chem. Res.*, 2021, **54**, 3083–3094.
19 N. Li, J. Xu, R. Feng, T.-L. Hu and X.-H. Bu, *Chem. Commun.*, 2016, **52**, 8501–8513.
20 R. E. Morris and L. Brammer, *Chem. Soc. Rev.*, 2017, **46**, 5444–5462.
21 A. Schoedel, M. Li, D. Li, M. O'Keeffe and O. M. Yaghi, *Chem. Rev.*, 2016, **116**, 12466–12535.
22 J. L. C. Rowsell and O. M. Yaghi, *J. Am. Chem. Soc.*, 2006, **128**, 1304–1315.
23 S. R. Caskey, A. G. Wong-Foy and A. J. Matzger, *J. Am. Chem. Soc.*, 2008, **130**, 10870–10871.
24 R. Sanz, F. Martínez, G. Orcajo, L. Wojtas and D. Briones, *Dalton Trans.*, 2013, **42**, 2392–2398.
25 W. L. Queen, M. R. Hudson, E. D. Bloch, J. A. Mason, M. I. Gonzalez, J. S. Lee, D. Gygi, J. D. Howe, K. Lee, T. A. Darwish, M. James, V. K. Peterson, S. J. Teat, B. Smit, J. B. Neaton, J. R. Long and C. M. Brown, *Chem. Sci.*, 2014, **5**, 4569–4581.
26 N. L. Rosi, J. Kim, M. Eddaoudi, B. Chen, M. O'Keeffe and O. M. Yaghi, *J. Am. Chem. Soc.*, 2005, **127**, 1504–1518.
27 K. Barthelet, J. Marrot, D. Riou and G. Férey, *Angew. Chem., Int. Ed.*, 2002, **41**, 281–284.
28 H. Reinsch, M. A. van der Veen, B. Gil, B. Marszalek, T. Verbiest, D. de Vos and N. Stock, *Chem. Mater.*, 2012, **25**, 17–26.
29 H. Reinsch and D. De Vos, *Microporous Mesoporous Mater.*, 2014, **200**, 311–316.
30 Y. Zhang, B. E. G. Lucier, S. M. McKenzie, M. Arhangelskis, A. J. Morris, T. Friščić, J. W. Reid, V. V. Terskikh, M. Chen and Y. Huang, *ACS Appl. Mater. Interfaces*, 2018, **10**, 28582–28596.
31 K. Barthelet, J. Marrot, G. Férey and D. Riou, *Chem. Commun.*, 2004, 520–521.
32 X. Qian, B. Yadian, R. Wu, Y. Long, K. Zhou, B. Zhu and Y. Huang, *Int. J. Hydrogen*, 2013, **38**, 16710–16715.
33 M. A. van der Veen, S. Canossa, M. Wahiduzzaman, G. Nenert, D. Frohlich, D. Rega, H. Reinsch, L. Shupletsov, K. Markey, D. E. De Vos, M. Bonn, N. Stock, G. Maurin and E. H. G. Backus, *Adv. Mater.*, 2023, e2210050.
34 S. Couck, J. F. M. Denayer, G. V. Baron, T. Rémy, J. Gascon and F. Kapteijn, *J. Am. Chem. Soc.*, 2009, **131**, 6326–6327.
35 A. López-Olvera, J. A. Zárate, E. Martínez-Ahumada, D. Fan, M. L. Díaz-Ramírez, P. A. Sáenz-Cavazos, V. Martis, D. R. Williams, E. Sánchez-González, G. Maurin and I. A. Ibarra, *ACS Appl. Mater. Interfaces*, 2021, **13**, 39363–39370.
36 Y. Wu, T. Yan, W. Zhang, S. Chen, Y. Fu, Z. Zhang and H. Ma, *Ind. Eng. Chem. Res.*, 2022, **61**, 13603–13611.
37 M.-B. Kim, T.-H. Kim, T.-U. Yoon, J. H. Kang, J.-H. Kim and Y.-S. Bae, *J. Ind. Eng. Chem.*, 2020, **84**, 179–184.
38 M.-B. Kim, S.-J. Lee, C. Y. Lee and Y.-S. Bae, *Microporous Mesoporous Mater.*, 2014, **190**, 356–361.
39 M.-B. Kim, T.-U. Yoon, D.-Y. Hong, S.-Y. Kim, S.-J. Lee, S.-I. Kim, S.-K. Lee, J.-S. Chang and Y.-S. Bae, *Chem. Eng. J.*, 2015, **276**, 315–321.
40 M.-B. Kim, K.-M. Kim, T.-H. Kim, T.-U. Yoon, E.-J. Kim, J.-H. Kim and Y.-S. Bae, *Chem. Eng. J.*, 2018, **339**, 223–229.
41 L. Yan, H.-T. Zheng, L. Song, Z.-W. Wei, J.-J. Jiang and C.-Y. Su, *Chem. Eng. J.*, 2023, **472**, 145145.
42 S.-T. Zheng, R.-Y. Jiang, Y. Jiang, S. Ni, G.-W. Guan, S.-Q. Shao, Y.-C. Wang, S.-M. Wang and Q.-Y. Yang, *Sep. Purif. Technol.*, 2023, **318**, 123957.
43 S.-M. Wang, X.-T. Mu, H.-R. Liu, S.-T. Zheng and Q.-Y. Yang, *Angew. Chem., Int. Ed.*, 2022, **61**, e202207066.
44 J. Ren, M. Chang, W. Zeng, Y. Xia, D. Liu, G. Maurin and Q. Yang, *Chem. Mater.*, 2021, **33**, 5108–5114.
45 K. C. Stylianou, R. Heck, S. Y. Chong, J. Basca, J. T. A. Jones, Y. Z. Khimyak, D. Bradshaw and M. J. Rosseinsky, *J. Am. Chem. Soc.*, 2010, **132**, 4119–4130.
46 A. Cadiau, N. Kolobov, S. Srinivasan, M. G. Goesten, H. Haspel, A. V. Bavykina, M. R. Tchalala, P. Maity, A. Goryachev, A. S. Poryvaev, M. Eddaoudi, M. V. Fedin, O. F. Mohammed and J. Gascon, *Angew. Chem., Int. Ed.*, 2020, **59**, 13468–13472.
47 M. Krüger, R. Siegel, A. Dreischarf, H. Reinsch, J. Senker and N. Stock, *Microporous Mesoporous Mater.*, 2015, **216**, 27–35.

48 P. Rönfeldt, H. Reinsch, M. P. M. Poschmann, H. Terraschke and N. Stock, *Cryst. Growth Des.*, 2020, **20**, 4686–4694.
49 Y. An, X. Lv, W. Jiang, L. Wang, Y. Shi, X. Hang and H. Pang, *Green Chem. Eng.*, 2023, DOI: **10.1016/j.gce.2023.07.004**.
50 S. Gai, J. Zhang, R. Fan, K. Xing, W. Chen, K. Zhu, X. Zheng, P. Wang, X. Fang and Y. Yang, *ACS Appl. Mater. Interfaces*, 2020, **12**, 8650–8662.
51 M. Chang, T. Yan, Y. Wei, J.-X. Wang, D. Liu and J.-F. Chen, *Chem. Mater.*, 2022, **34**, 9134–9143.
52 J. A. Dunne, M. Rao, S. Sircar, R. J. Gorte and A. L. Myers, *Langmuir*, 1996, **12**, 5896–5904.
53 T. Düren, Y.-S. Bae and R. Q. Snurr, *Chem. Soc. Rev.*, 2009, **38**, 1237–1247.
54 F. R. Siperstein, C. Avendaño, J. J. Ortiz and A. Gil-Villegas, *AIChE J.*, 2021, **67**, e17186.
55 D. Fröhlich, S. K. Henninger and C. Janiak, *Dalton Trans.*, 2014, **43**, 15300–15304.
56 S. Devautour-Vinot, G. Maurin, F. Henn, C. Serre and G. Férey, *Phys. Chem. Chem. Phys.*, 2010, **12**, 12478–12485.
57 F.-X. Coudert, A. U. Ortiz, V. Haigis, D. Bousquet, A. H. Fuchs, A. Ballandras, G. Weber, I. Bezverkhyy, N. Geoffroy, J.-P. Bellat, G. Ortiz, G. Chaplais, J. Patarin and A. Boutin, *J. Phys. Chem. C*, 2014, **118**, 5397–5405.
58 M. J. Kalmutzki, C. S. Diercks and O. M. Yaghi, *Adv. Mater.*, 2018, **30**, e1704304.